Hindawi
Advances in Materials Science and Engineering
Volume 2022, Article ID 6360301, 12 pages
https://doi.org/10.1155/2022/6360301

Research Article

Characteristics of Pavement Cement Concrete Incorporating Steel Slag Powder

Erbu Tian,[1,2] **Yamin Liu**,[3] **Xianpeng Cheng**,[4] **and Wuhua Zeng**[1,2]

[1]*School of Civil Engineering, Sanming University, Sanming 365004, China*
[2]*Key Laboratory of Engineering Material & Structure Reinforcement in Fujian Province, Sanming 365004, China*
[3]*Key Laboratory for Special Area Highway Engineering of Ministry of Education, Chang'an University, Xi'an 710064, China*
[4]*Xi'an University of Finance and Economics, Xi'an 710100, China*

Correspondence should be addressed to Erbu Tian; testb@fjsmu.edu.cn

Received 16 August 2021; Revised 23 March 2022; Accepted 6 May 2022; Published 27 June 2022

Academic Editor: Bo Li

After thermal braising and magnetic separation, steel slag is often ground into steel slag powder (SSP), which contains active silica (SiO_2) and can be used as a cementitious material to replace part of the cement and applied in concrete. However, there have been relatively few studies on the influence of SSP on the performance of pavement cement concrete (PCC). In this paper, SSP was used as an admixture to replace part of the cement in the cement paste, cement mortar, and PCC, to investigate the effect of SSP on the fluidity of SSP-cement slurry, the mechanical properties, and the durability of PCC. Results showed that SSP can lead to the secondary hydration reaction with $Ca(OH)_2$ in the cement paste and affect the hydration products, morphology, pore characteristics, and strength of the cement paste. When the SSP mixing amount was less than 20% and up to 1.3% superplasticizer was added, the fluidity of the cement slurry could be optimized. For the samples with the SSP mixing amount of less than 20%, the concrete compressive strengths were greater than 50 MPa, and the flexural strengths were greater than 5.0 MPa. As the SSP mixing amount increased, concrete displayed a better anticarbonization performance. Finally, using 15% SSP, the best performance in terms of the concrete antipermeability (chloride ion diffusion coefficient and electric flux) and frost resistance was achieved.

1. Introduction

Steel slag (SS) is one of the typical industrial wastes in steel production, characterized by abundant free calcium/magnesium oxide, low cementitious properties, and high heavy metal contents. While manufacturing one ton of steel, 130 ~ 200 kg SS is produced as byproducts [1, 2]. In 2020, the amount of SS was estimated to be between 180 and 270 million tons globally [3]. The SS disposal in the landfill without applying is obviously wasteful and would also cause pollution to the environment.

Recently, many studies have focused on using SS as an ecofriendly material, particularly as a cementitious material. Usually, the SS comprise 45%–60% calcium oxide (CaO), 10%–15% silicon dioxide (SiO_2), 7%–20% iron trioxide (Fe_2O_3), 3%–13% magnesium oxide (MgO), 1%–8% manganese oxide (MnO), 1%–7% aluminum oxide (Al_2O_3), and phosphorous pentoxide 1%–4% (P_2O_5) [4, 5]. The SSs contain the same mineral compositions as cement, such as C_3S, C_2S, C_4AF, and C_2F, which are potential mineral admixtures in the cement or concrete industry [4, 6, 7]. After thermal braising and magnetic separation, the substances that affect the SS stability (free CaO and MgO) are greatly reduced, and the difficulty in grinding due to a large amount of iron minerals is solved [8, 9].

SS is frequently utilized as asphalt pavement material on highways for its high strength. In this respect, Morisson [10] used SS to prepare the mixture of 50% SS, 39% stream sand, 3% fly ash, and 8% asphalt cement, which could render service at places with no heavy truck traffic for longer than 10 years without structural deformation. Moreover, the SS is also employed as the railway ballast, leading to three essential effects, i.e., spreading vertical loads, providing elasticity to the rails, and preventing plant growth [11]. In research by Palankar et al. [12], SS was exploited in concrete instead of 50% coarse aggregate to improve the compressive

Table 1: Chemical compositions of the cement and SSP (%).

Samples	CaO	SiO_2	Al_2O_3	Fe_2O_3	MgO	MnO	P_2O_5	SO_3	Na_2O_{eq}	Loss
Cement	56.11	23.46	7.93	3.46	3.15	–	–	3.49	0.72	2.31
SSP	44.57	18.11	7.26	19.01	4.17	2.55	1.87	–	0.29	1.38

$Na_2O_{eq} = Na_2O + 0.685\ K_2O$.

strength, with the best results being about 60 MPa (very similar to the reference sample). In addition, the water absorption value increased, depending on the slag porosity.

SS is often ground into steel slag powder (SSP), and SSP can be used as a cost effective waste product in concrete [13] or an active additive in the secondary hydration reaction [14, 15]. Li et al. [16] used SSP to replace 10% of cement by mass, and the results showed that compressive strength was reduced with increasing the SSP mixing amount. SSP could also control the hydration process in high-performance concrete, although its early age strength was low.

SSP can also be utilized as an active admixture due to its filling characteristics and pozzolan activity. Li et al. [17] studied the effect of SSP on the low-temperature fracture performance of asphalt materials. Jiao et al. [18] found that SSP could improve the thermal conductivity of SSP asphalt concrete. Chaurand et al. [19] reused SSP as an aggregate for road constructions.

The iron content of the cement clinker affects the flexural strength of the cement, which is lower than that of the steel slag. It is unclear if SSP addition to the cement increases the flexural strength of the cement and improves the flexural performance of pavement cement concrete (PCC). The production of one ton of cement produces 765 kg CO_2, and the production of one ton of SSP produces 86 kg CO_2 [20]. If feasible, SSP will help reduce the amount of the cement in PCC and carbon emissions from pavement engineering, which is crucial.

In this paper, SSP was used as an admixture to replace a part of the cement in cement paste, cement mortar, and PCC, to study the influence of SSP on the fluidity of SSP-cement slurry, and the mechanical properties and durability of PCC.

2. Materials and Methods

2.1. Raw Materials. The ordinary Portland cement was used, with a specific surface area of 340 $m^2\ kg^{-1}$, and the strength grade of 42.5, and the technical indicators of cement were compiled according to ASTM C150/C150M-2012. Table 1 shows the chemical compositions of cement and SSP. The X-ray diffraction (XRD) pattern of the SSP is demonstrated in Figure 1. SSP produced by Fujian Sangang (Group) Co., Ltd. has been heat-simmered and magnetically separated, possessing a specific surface area of 456 kg m^{-2}.

After the heat-simmering and magnetic separation, the chemical compositions of SSP were dicalcium silicate (C_2S), tricalcium silicate (C_3S), calcium hydroxide ($Ca(OH)_2$), hydration calcium silicate (C–S–H), RO phase, silicon dioxide (SiO_2), calcium aluminum garnet ($Ca_2A_{l2}Si_3O_{12}$), calcium magnesium silicate (C-M-S), and iron aluminum calcium phase ($Ca_2(Fe, Al)_2O_5$), which are similar to those of

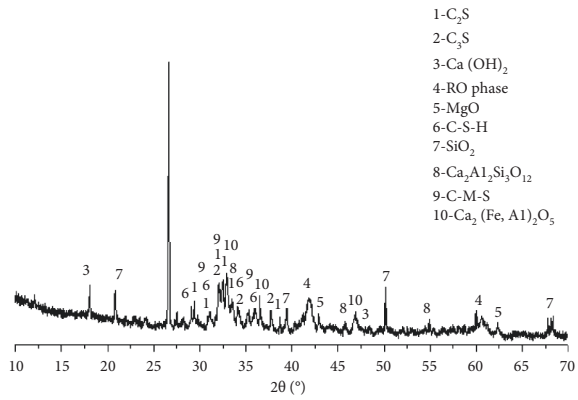

Figure 1: The XRD pattern of the steel slag.

cement. However, the formation temperature of SS was higher than that of the Portland cement clinker, so SS was also called overburned Portland cement [21]. The physical morphology of SSP is shown in Figure 2, in which the continuity of the particle size distribution of SSP was poor, and the SSP shape was irregular, comprising irregular quadrilateral, amorphous, and spherical. The contents of Mg, Mn, and Fe, shown as 1, 6, 9, and 10 marks in Figure 2, were relatively higher, showing that these SSP particles were RO phase, while the particle size of the similar cement clinker in SSP was smaller.

The coarse aggregate that was crushed basalt between 5 and 25 mm came from local quarries. The fine aggregate was natural river sand, smaller than 5 mm. The superplasticizer produced by Shandong Tengwei New Building Materials Co., Ltd. was used to achieve the desired workability for all cement slurry and concrete mixtures. All materials met the requirements of the related ASTM standards.

2.2. Mixture Design. SSP was used to replace some cement as the cementitious material. In this paper, the effects of three amounts of SSP (10, 15, and 20% by the weight of both SSP and cement) on the cement paste properties were investigated.

The details of the mixture design of the cement paste fluidity are shown in Table 2. The dose of superplasticizer was 0.4%, 0.6%, 0.8%, 0.9%, 1.0%, 1.1%, 1.2%, 1.3%, 1.4%, and 1.5% by the weight of cementitious material (both SSP and cement).

The details of the mixture design of the cement mortar are shown in Table 3.

The details of the mixture design of concrete are shown in Table 4. The dose of superplasticizer was 1.3% by the weight of cementitious material (both SSP and cement).

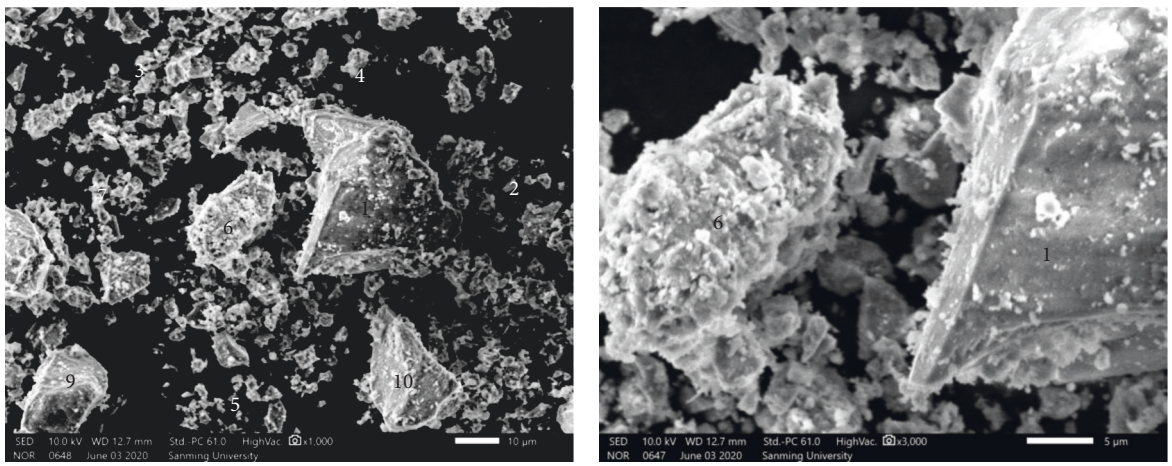

(a) (b)

Figure 2: Particle morphology of SSP. (a) Magnify 1000 times. (b) Magnify 3000 times.

Table 2: Mix proportions of the fluidity of cement paste.

Samples	Mix proportion (g)		Superplasticizer (%)										
	Cement	SSP											
C-P (100 : 0)	300	0	0	0.4	0.6	0.8	0.9	1.0	1.1	1.2	1.3	1.4	1.5
C-P (90 : 10)	270	30	0	0.4	0.6	0.8	0.9	1.0	1.1	1.2	1.3	1.4	1.5
C-P (85 : 15)	255	45	0	0.4	0.6	0.8	0.9	1.0	1.1	1.2	1.3	1.4	1.5
C-P (80 : 20)	240	60	0	0.4	0.6	0.8	0.9	1.0	1.1	1.2	1.3	1.4	1.5

Note. C-P (100 : 0) is the standard sample without SSP; the last number (C-P(80 : 20)) refers to the percentage of SSP in cementitious material (both SSP and cement), and so on.

Table 3: Mix proportions of cement mortar (g).

Samples	Cement	SSP	Water	Standard sand
CM-0	450	-	225	1350
CM-10	405	45		
CM-15	382.5	67.5		
CM-20	360	90		

Note. CM-0 is the standard sample without SSP; the number (CM-20) refers to the percentage of SSP in cementitious material (both SSP and cement), and so on.

Table 4: Mix proportions of concrete ($kg * m^{-3}$).

Samples	Cement	SSP	Water	Sand	Coarse aggregate	Superplasticizer
C-0	390	-	144	597	1269	5.07
C-10	351	39				
C-15	331.5	58.5				
C-20	312	78				

Note. C-0 is the standard sample without SSP; the number (C-20) refers to the percentage of SSP in cementitious material (both SSP and cement), and so on.

2.3. Test Methods

2.3.1. The Test Method of Cement Paste Fluidity. When SSP was added, first, the SSP and cement must have been mixed and stirred slowly for 30 s, and then 105 g water was added to test the cement paste fluidity according to ASTM C 311-2000.

2.3.2. The Test Methods of Cement Paste Hydration Properties. The pastes were cast in plastic sealed tubes after preparation, in case of water loss and carbonization, and were then cured at a temperature of 20°C ± 1°C. Hardened pastes were extracted and then immersed in absolute alcohol to prevent further hydration at testing ages. The samples were dried before testing using an electric vacuum drying oven.

(1) XRD Analysis. The Delong-7 X diffractometer manufactured in Germany was used to determine the mineral phases of the hydration products at the ages of 7, 28, and 180 d. The main technical parameters of the instrument are

as follows: tube voltage 0–60 kV, tube current 0–80 mA, the mode of continuous scanning, scanning speed 5°/min, and 2θ in the range (10°–80°).

(2) Morphology Analysis. The XL30 ESEM manufactured by FEI in the Netherlands was used to analyze the micromorphology of the cement paste under a high vacuum at the ages of 3, 7, 28, and 180 d. The accelerating voltage was 15–20 kV, and the working distance was 10 mm. A magnification of 2000 was selected for the analyses. The energy dispersive spectrometer was used to analyze the chemical elements of hydration products of the cement paste under a high vacuum at the ages of 3, 28, and 180 d.

(3) Pore Analysis. The pore characteristics of paste at the ages of 180 d were determined by dynamic nitrogen adsorption using the 3H-2000PS Beishide Instrument according to ASTM D 4365-2013.

2.3.3. The Test Method of Cement Mortar Strength. The standard sand of the cement mortar was consistent with the requirements of 5.1.3 in ISO 679: 2009. When the cement mortar would be mixed, the cement and SSP were added to the mixing pot together. Cement mortars of 40 mm × 40 mm × 160 mm were cast, then covered with the mold and placed on a horizontal shelf in a humidity curing box for curing for 24 hours, and removed the mold. Then, they were put in the water with a temperature of 20°C ± 1°C. The cement mortar strength tests were conducted in accordance with ASTM C 109/C 109M-2001 at the ages of 3, 7, 28, and 180 d.

2.3.4. The Test Method of Concrete Strength. Specimens of 150 mm × 150 mm × 150 mm and 150 mm × 150 mm × 550 mm were cast. Specimens were cured in a room with a temperature of 20°C ± 2°C and relative humidity of higher than 95%. The compressive strength and flexural strength of concrete were measured in accordance with ASTM C 293-2002 at the ages of 7 d and 28 d.

2.3.5. The Test Methods of Concrete Durability

(1) Chloride Ion Permeability. The concrete chloride ion permeability was tested at the age of 28 d and evaluated by measuring the current passing through the concrete, according to ASTM C 1202.

(2) Carbonation Resistance. Specimens of 100 mm × 100 mm × 100 mm were cast, and at the age of 26 d, the specimens were taken out of the standard curing condition and baked at 60°C for 48 hours and then were placed in a chamber with a temperature of 20°C ± 2°C, relative humidity of 70% ± 5% and a carbon dioxide concentration of 20% ± 3% for accelerated carbonation according to the ASTM C 1202. The carbonation depths of the specimens were tested after accelerated carbonation for 3, 7, and 28 d. Finally, the carbonation depth of concrete incorporating SSP could be calculated by

$$\overline{d_t} = \frac{1}{n}\sum_{i=1}^{n} d_i, \tag{1}$$

where $\overline{d}_t$ = average carbonization depth (mm); d_i = carbonization depth of a measuring point; n = total number of measuring points.

(3) Frost Resistance. The preparation procedure and size of the specimens in this test were consistent with the carbonization test. The difference was the curing method of the specimens. Before testing according to the ASTM C 1202, the specimens were cured for 24 days in standard conditions. Subsequently, the specimens were soaked for 4 days in water at 20°C ± 2°C, and the water surface was at least 20 mm higher than the specimens. A freeze-thaw cycle test was performed after curing. The mass loss of the specimens per 50 freeze-thaw cycles was recorded. Once the mass loss exceeded 5%, the test was terminated.

3. Results and Discussion

3.1. The Fluidity of Cement Paste. Figure 3 shows the fluidity changing curves with the increase of superplasticizer amount, when the SSP mixing amounts were 0%, 10%, 15%, and 20% (20 wt.% of both cement and SSP), respectively. Regardless of the SSP mixing amount, the fluidity of the cement paste increased with the increase in the superplasticizer amount and eventually leveled out. When the SSP mixing amounts were 0%, 10%, 15%, and 20%, the mixing amounts of superplasticizer that reached the maximum fluidity of the cement paste were significantly different, 3.0, 3.6, 3.9, and 3.9 g, respectively. It shows that as the SSP mixing amount increases, the fluidity of the slurry is decreased, mainly because the specific surface area of SSP is greater than that of cement. The SSP was finer than cement, and the water attraction was greater. More hydrophobic functional groups were needed to disperse the SSP particles, so a higher superplasticizer amount must have been added. The mixing amount of SSP was within 20%, and the superplasticizer amount in subsequent tests was 3.9 g (that is, 1.3% of the mass of the cementitious material) to ensure that the test could reach the maximum fluidity.

3.2. The Hydration Properties of Cement Paste

3.2.1. XRD Analysis. Figure 4 shows XRD patterns of cement paste with ages of 7, 28, and 180 d, when the mixing amount of SSP was 20%. According to the analysis results shown in Figure 4, the main minerals in the paste were hydrated C–S–H gel and $Ca(OH)_2$, residual minerals and the RO phase of SSP, and some unreacted gelling mineral silicates. Compared with the XRD pattern of the age of 7 d, the peaks of silicon oxide and calcium hydroxide for ages of 28 d and 180 d generally tend to decreased. This is due to the fact that the amorphous SiO_2 with lattice defects, which is the active SiO_2, reacts with $Ca(OH)_2$ in the solution for

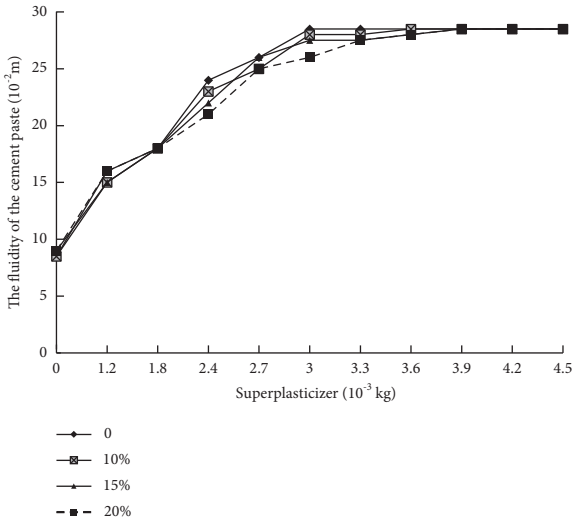

Figure 3: The fluidity change of the cement paste with the superplasticizer amount.

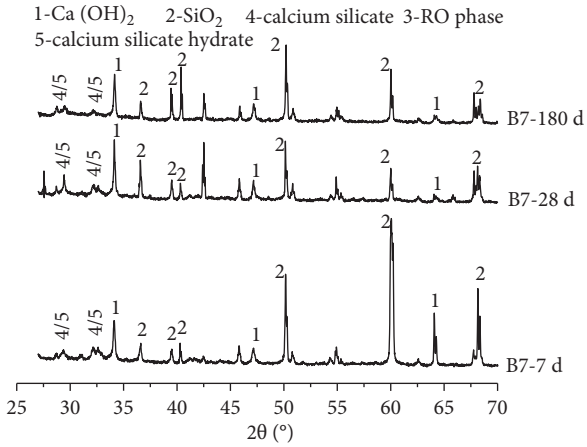

Figure 4: XRD patterns of the cement paste with 20% SSP.

secondary hydration. The secondary hydration is specifically a cement paste mixed with SSP. It provides an alkaline environment during the cement hydration, which can stimulate the activity of SSP and accelerate the generation rate of SSP hydration products. When the concentration of calcium hydroxide in the slurry reaches a certain level, it will react with the active SiO_2 to produce C–S–H.

3.2.2. Morphology Analysis. Figures 5–7 show the microscopic morphology images of cement pastes with ages of 3, 28, and 180 d, respectively, when the mixing amount of SSP was 20%, and the energy spectrum analysis of the corresponding regions is also displayed. Figure 5(a) demonstrates that there were more hydration products, and unhydrated particles were encapsulated by the hydration products. Figures 5(b) and 5(d) of the energy spectrum analysis chart show that the main chemical components of the regions Spc_3d_B2-4 and Spc_3d_B2-6 were O, Si, Al, and Ca, which should be unhydrated gelling components, calcium aluminum garnet ($Ca_2Al_2Si_3O_{12}$). Figure 7(d) of the energy spectrum analysis chart also indicates that the main chemical components of the area Spc_180d_B7-3 were O, Si, Al, and Ca. Whether in the early or later stage of hydration, $Ca_2Al_2Si_3O_{12}$ was formed in the micromorphology of the SSP-cement paste. It can be seen that the $Ca_2Al_2Si_3O_{12}$, with a smooth surface and large-particle size, was not easy to hydrate.

Figures 6(a) and 6(c) had a higher gel amount in the hardened paste than Figures 5(a) and 5(c), respectively, with an age of 180 d, and the paste structure was very dense. From Figures 7(a) and 7(c), it can be observed that there were particles with a complete shape, which were embedded between the gel-like hydration products, but there were weak connections between some larger particles and the surrounding hydration products. Most of the particles with smooth a surface and large-particle sizes were the RO phase of the SSP. The energy spectrum analysis in Figures 7(b) and 7(f) also shows that the components of the area Spc_180d_B7-1 and the area Spc_180d_B7-4 were O and Mg, which belong to the RO phase. Geiseler et al. [22] revealed that the hydration reaction ability of the RO phase depends on its composition. When the MgO content in the RO phase is sufficient, this RO phase type will have certain hydration activity. Two RO phases can be found in Figures 6 and 7; one type is shown in Figures 7(a) and 7(e), in which the RO phases were larger, and the RO phase surface was smooth since they did not participate in the chemical reaction. The other type is shown in Figure 6(a), in which the RO phases were relatively small and the RO phase surface was rough. The RO phase size was about 5 um and a chemical reaction occurred on the RO phase surface. The energy spectrum analysis results are shown in Figures 6(b) and 6(d). The area Spc_28d_B7-2 mainly contained O and Mg, and the area Spc_28d_B7-3 mostly comprised O, Si, and Ca. There was C–S–H gel on the RO phase, indicating that the RO phase had begun to undergo the hydration reaction. Therefore, the RO phase with a small particle size, in addition to being active due to the high content of MgO and participating in the hydration reaction, can also fill the pores left by water consumption or loss in the hardened paste, and play a role in filling microaggregates. Due to its smooth surface and weak bonding with the surrounding gel, the RO phase with a larger particle size may form a weak link in the hardened paste.

Figures 8(a) and 8(b) show the microscopic morphology of cement paste with 20% SSP at the age of 7 d. It can be clearly seen from Figure 8(b) that hexagonal plate-like crystals with regular shapes were formed, named calcium aluminate hydrate, which was in a metastable state at room temperature, also commonly known as cubic hydrogarnet (C_3AH_6). According to Bensted and Barnes [23], C_3AH_6 can be obtained in two ways: one is produced by CA hydration reaction at a temperature higher than 60°C, and the other is produced by mayenite ($C_{12}A_7$) hydration at room temperature to produce C_3AH_6 and C_2AH_8. Figure 8(a) shows that there was a large amount of calcium aluminate hydrate and "catkins" hydration products, and a crack can be clearly seen, indicating that the strength of the hydration products in this state was low.

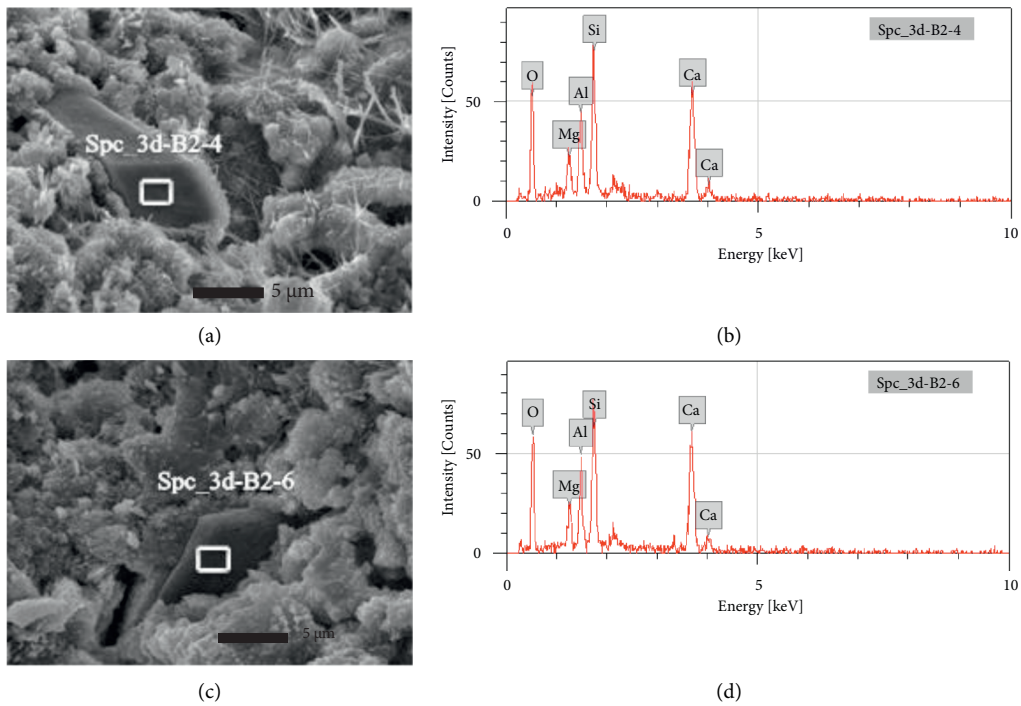

Figure 5: SSP-cement hydration microscopic morphology and energy spectrum analysis with the age of 3 d: (a) hydration microstructure with age of 3 d, (b) energy spectrum analysis of area Spc_3d_B2-4, (c) hydration microstructure with age of 3 d, and (d) energy spectrum analysis of area Spc_3d_B2-6.

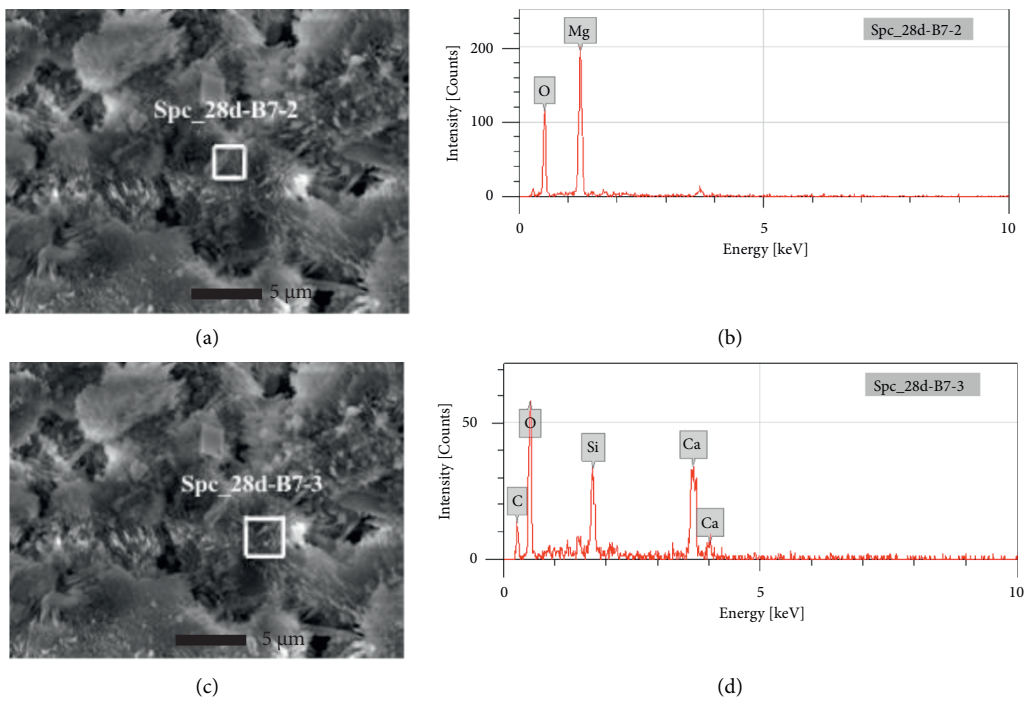

Figure 6: SSP-cement hydration microscopic morphology and energy spectrum analysis with the age of 28 d: (a) hydration microstructure with age of 28 d, (b) energy spectrum analysis of area Spc_28d_B7-2, (c) hydration microstructure with age of 28 d, and (d) energy spectrum analysis of area Spc_28d_B7-3.

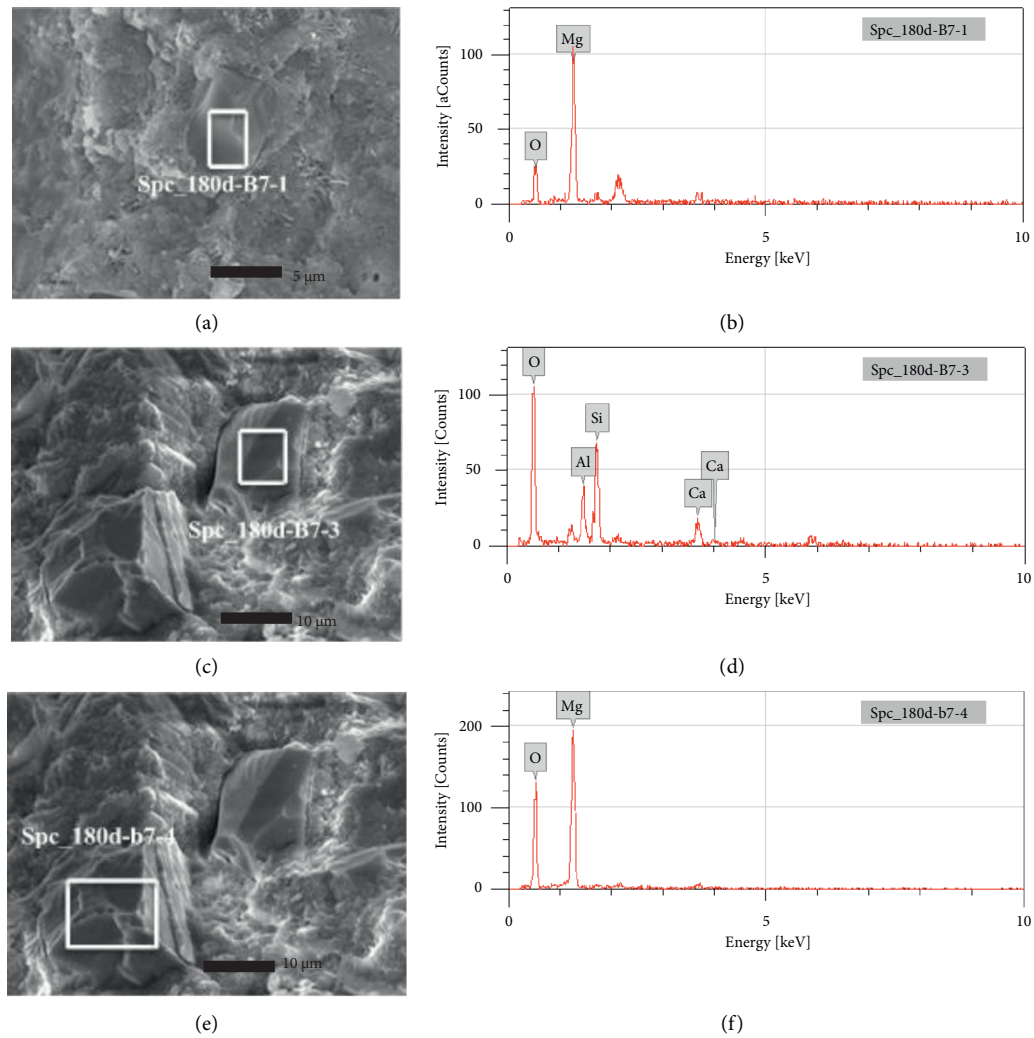

Figure 7: SSP-cement hydration microscopic morphology and energy spectrum analysis with the age of 180 d, (a) hydration microstructure with age of 180 d, (b) energy spectrum analysis of area Spc_180d_B7-1, (c) hydration microstructure with age of 180 d, (d) energy spectrum analysis of area Spc_180d_B7-3, (e) hydration microstructure with age of 180 d, and (f) energy spectrum analysis of area Spc_180d_B7-4.

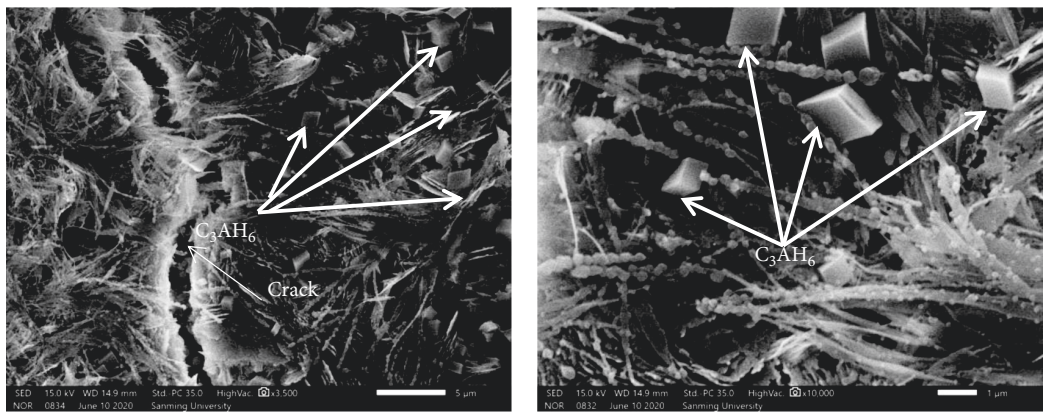

Figure 8: SSP-cement hydration microscopic morphology with the age of 7 d: (a) magnify 3500 times and (b) magnify 10000 times.

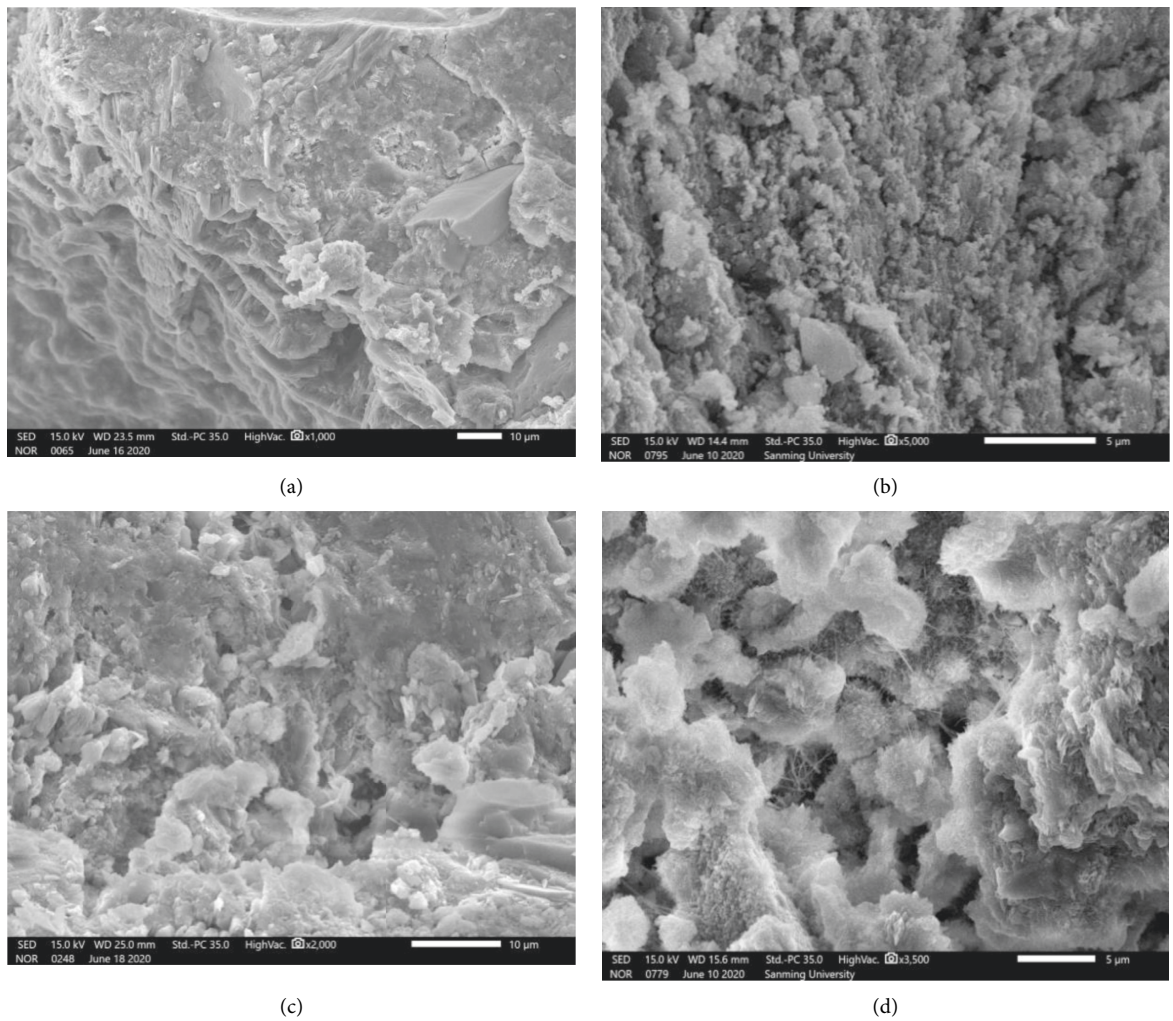

Figure 9: The microscopic morphology with the age of 7 d, (a) 0% steel slag powder mixed amount, 15% steel slag powder mixed amount, (b) 10% steel slag powder mixed amount, (c) 15% steel slag powder mixed amount, and (d) 20% steel slag powder mixed amount.

Figures 9(a)–9(d) demonstrate the microscopic morphology of the hardened cement paste with different SSP mixing amounts at the age of 7 d. The hydration products of the paste were very different. Figure 9(a) displays the plain cement (C-0) without SSP. Its hydration products of C–S–H gel and C-H phase were more, and the structures were very dense, and the pores were less. Figure 9(b) shows the microscopic morphology of the cement paste containing 10% SSP. Its hydration products formed a stable microstructure with fewer pores and a higher density, and the C–S–H gel was connected as a whole. Figure 9(d) shows the microscopic morphology of the cement paste containing 20% SSP, with fewer hydration products, no prismatic $Ca(OH)_2$, loose structure, many pores, and poor compactness. The strength test results of the paste with SSP also showed the corresponding characteristics. The strength of the mortar decreased with the increase of the SSP mixing amounts, and when the mixing amount was 20%, the strength of the mortar sand was further decreased. It can be seen that an increase in the SSP mixing amount could increase the pores of the hardened paste, resulting in a poorly compact structure, which is not effective in enhancing the paste strength.

3.2.3. Pore Analysis. Studies [24, 25] have shown that the pore size distribution can significantly affect the mechanical properties of hardened cement pastes. There are different types according to the aperture size. Gel pores are connected pores of gel particles with a pore diameter of less than 10 nm, which are harmless. Transition pores are regarded as pores between external hydration products, with a pore diameter between 10 and 50 nm, which are less harmful pores. Capillary pores are the original water-filled spaces that are not filled by hydration products, and their size is greater than 100 nm, which are harmful pores. Table 5 shows the ratio of the pore size distribution of cement paste at the age of 180 d. SSP greatly changed the pore size distribution ratio. Because the SSP particles are finer than cement, they could fill the capillary pores. Moreover, SSP participated in the secondary hydration reaction and improved the transition pores.

Table 5: The ratio of the pore size distribution (%).

Samples	Pore size					
	<10 nm	10–20 nm	20–50 nm	50–100 nm	100–200 nm	>200 nm
C-0	12.24	19.19	35.95	16.31	13.51	2.79
C-10	15.61	20.11	34.15	19	11.13	0
C-15	23.99	19.89	35.21	13.21	8.7	0
C-20	18.31	11.15	26.75	19.29	21.35	3.15

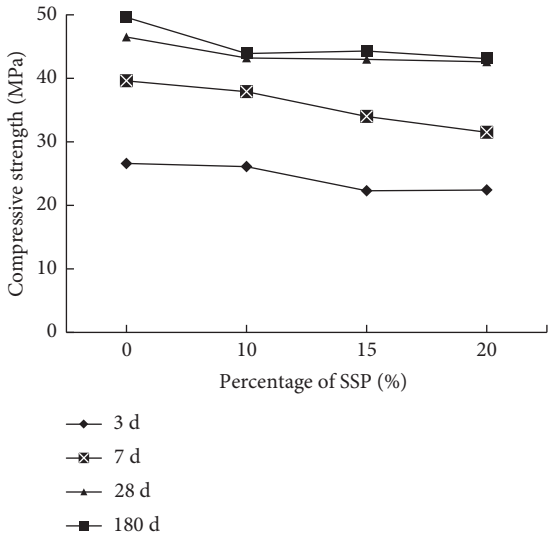

Figure 10: The compressive strength of mortar.

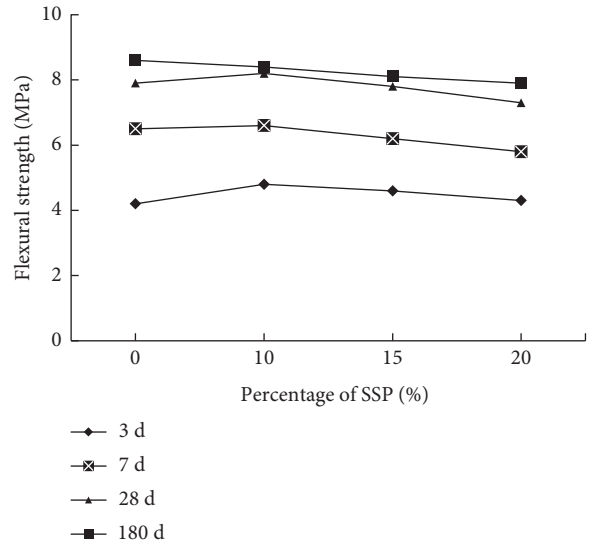

Figure 11: The flexural strength of mortar.

3.3. Strength

3.3.1. The Strength of Cement Mortar. Figures 10 and 11 plot the effect of the SSP mixing amount on the compressive and flexural strengths of cement mortars. It can be seen from Figures 10 and 11 that the longer the age, the higher the curve position, indicating the increase in the curing time, the compressive, and flexural strength of cement mortar. However, for the same curing time, with increasing the SSP mixing amount, the compressive and flexural strengths of cement mortar fluctuated in a small range, but the overall trend was downward. When the curing time was from 7 d to 180 d, with raising the SSP mixing amount, the overall compressive strength and flexural strength of cement mortar increased greatly, indicating that during the age from 28 d to 180 d, SSP participated in the secondary hydration reaction, and increased the compressive and flexural strength of the cement mortar.

3.3.2. The Strength of Concrete

(1) Flexural Strength. It can be seen from Figure 12 that when the standard curing age was 7 d, the flexural strengths of concrete mixed with SSP were lower than that of the C-0 concrete, and as the SSP mixing amounts increased, the flexural strengths gradually decreased, but the flexural strengths of each group were greater than 3.5 MPa, which meets the index requirements of the PCC flexural strength. As the curing age reached 28 d, the flexural strengths became greater than 5.0 MPa, reaching the specification requirements, and with the increase of the SSP mixing amounts, the flexural strengths of the concrete gradually decreased.

(2) Compressive Strength. Figure 13 shows that independent of the SSP addition amount, the compressive strengths of concrete increased with elongating the curing age. As the SSP mixing amounts increased, the compressive strengths of concrete showed a slightly decreasing trend. The compressive strengths of the SSP concrete increased rapidly in the later stage, mainly because the SSP participated in the secondary hydration reaction. In different curing ages, the concretes with 20% SSP showed higher compressive strengths, and when the curing age was 28 d, the compressive strengths of the different SSP mixing amounts reached more than 50 MPa, meeting the PCC specification requirements. It shows that the influence of the single SSP addition on the later compressive strength of concrete is small.

3.4. Durability

3.4.1. Chloride Ion Permeability. Table 6 shows the results of chloride ion permeability of the concretes. According to ASTM C1202, the grade of chloride ion permeability is "low" when the electric flux is between 1000 and 2000°C, and the grade is "moderate" when the electric flux is between 2000 and 4000 C. The permeability grades of C-0, C-10, and C-20 were medium, but the permeability grade of C-15 was low,

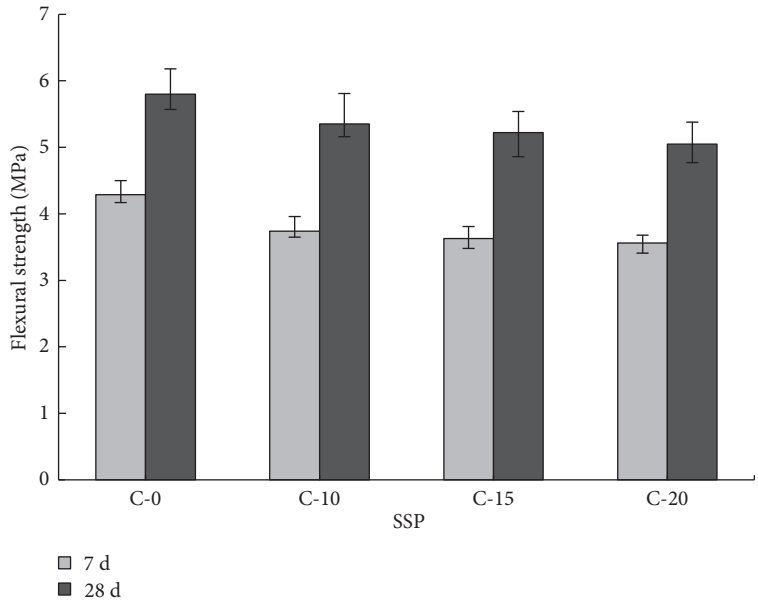

Figure 12: The flexural strength.

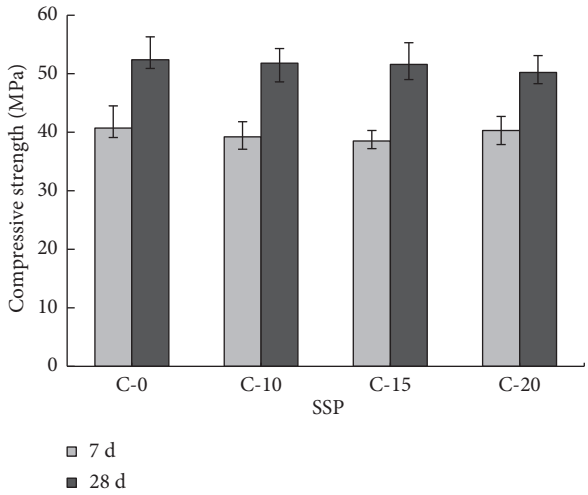

Figure 13: The compressive strength.

which was the lowest electric flux and the smallest chloride ion diffusion coefficient. Electric flux and chloride ion diffusion coefficients gradually decreased with the SSP mixing amount and then increased. When the SSP mixing amount was 15%, the two were the lowest. With increasing the SSP mixing amount, more and more SSP participated in the secondary hydration reaction, and the produced C–S–H gel could block the diffusion channel, improving the pore size distribution and geometric shape of the concrete pores; both the electric flux and the chloride ion diffusion coefficients were reduced. When the SSP mixing amount reached 15%, the electric flux was the lowest, and the chloride ion diffusion coefficient was the smallest. Combined with mechanical test results in Figures 12 and 13, it can be seen that an appropriate amount of SSP is beneficial in improving the pore structure of the concrete, increasing the concrete density, reducing the permeability, and improving the antipermeability performance of the concrete.

3.4.2. Carbonation Resistance. Figure 14 shows the carbonization depths of concrete with different mixing amounts of SSP and different carbonization times of 3, 7, and 28 d. The results show that as the mixing amounts of SSP increase, the anticarbonization effects of concrete are better. As the carbonization times increase, the overall carbonization depths of the concrete gradually increase, and the carbonization depths of the concrete with 0% and 10% SSP increase rapidly after carbonization for 7 d, while the increases are not much for concrete with 15% and 20% SSP. These results show that the $Ca(OH)_2$ produced by cement hydration have a secondary reaction with SSP, which reduces the $Ca(OH)_2$ production in the concrete and produces the C–S–H gel, and the SSP also fills the concrete pores and improves the pore size distribution and geometric shape of the concrete pores, and blocks some channels of concrete carbonization and reduces the chance of carbonization.

3.4.3. Frost Resistance. Table 7 shows the results of the weight and strength loss of concrete after freezing and thawing. After 100 freeze-thaw cycles, some shedding signs were found on the C-0 surface. After the 104th freeze-thaw cycle of the C-0, the mass loss reached 12%, and the strength dropped sharply by 36%. After 100 freeze-thaw cycles, the mass loss measurement and compressive strength test of C-0, C-10, C-15, and C-20 were performed. The results are given in Table 7, which show that before the freeze-thaw test, the apparent density of the C-15 concrete was the highest, and after 100 freeze-thaw cycles, the concrete with 15% SSP had the least mass loss and the lowest compressive strength loss. SSPs not only participated in the secondary hydration reaction but also had a filling effect, making the concrete

Table 6: The chloride ion permeability of concrete.

Samples	SSP	Electric flux (C)	Evaluation standard for the chloride ion permeability		Cl-diffusion coefficient (10^{-9} cm^2 s^{-1})
			Evaluation standard	Chloride ion permeability	
C-0	0	2444.2	2000–4000	Moderate	13.78
C-10	10%	2040.1	2000–4000	Moderate	12.61
C-15	15%	1877.91	2000–4000	Low	11.82
C-20	20%	2961.05	2000–4000	Moderate	17.15

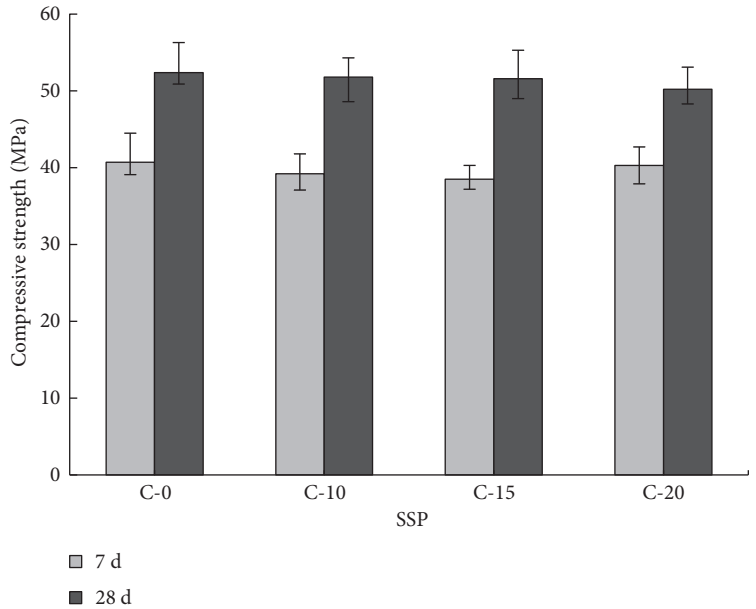

Figure 14: Carbonation depth of concrete.

Table 7: The weight and strength loss of concrete after freezing and thawing.

Samples	Mass (kg)			Compressive strength (MPa)		
	Before	After	Mass loss	Before	After	Strength loss
C-0	2.413	2.398	0.015	52.4	48.5	3.9
C-10	2.419	2.412	0.007	51.8	48.6	3.2
C-15	2.426	2.422	0.004	51.6	50	1.6
C-20	2.416	2.408	0.008	50.2	46.6	3.6

Note. The "Before" of compressive strength is the compressive strength of concrete at the age of 28 d, which is the 28 d compressive strength of Figure 13.

denser. The capillary channels of the concrete were filled with the C–S–H gel, and the products of the secondary hydration reaction made the pore size of the SSP-cement slurry smaller with fewer connecting holes. So, the water entering probability could be greatly reduced, decreasing the destroying chance of the concrete structure.

4. Conclusion

The SSP which possesses active SiO_2 can lead to the secondary hydration reaction with $Ca(OH)_2$ in the cement paste and affects the hydration products, morphology, pore characteristics, and strength of the cement paste.

When the mixing amount of SSP was less than 20% and the superplasticizer was added by 1.3% of the mass of the cementitious material, the fluidity of the cement slurry reached the maximum.

Within 20% SSP mixing amount, the concrete compressive strengths were greater than 50 MPa, and the flexural strengths were greater than 5.0 MPa, meeting the PCC specification requirements.

With increasing the SSP mixing amount, the concrete with a better anticarbonization performance was obtained. When the SSP mixing amount was 15%, the concrete antipermeability (chloride ion diffusion coefficient and electric flux) and frost resistance were the best.

Data Availability

The processed data required to reproduce these findings cannot be shared at this time as the data also form part of an ongoing study.

Conflicts of Interest

The authors declare that they have no conflicts of interest.

Acknowledgments

This work was supported by the Department of Science and Technology, Fujian Province, China (no. 2019Y0044). The authors thank Yuezong Lian and Haixin Kang for providing the steel slag sample.

References

[1] A. M. Rashad, "A synopsis manual about recycling steel slag as a cementitious material," *Journal of Materials Research and Technology*, vol. 8, no. 5, pp. 4940–4955, 2019.

[2] Q. Song, M.-Z. Guo, L. Wang, and T.-C. Ling, "Use of steel slag as sustainable construction materials: a review of accelerated carbonation treatment," *Resources, Conservation and Recycling*, vol. 173, Article ID 105740, 2021.

[3] U.S. Geological Survey, "Mineral commodity summaries 2021," *Mineral Commodity Summaries*, 2021.

[4] S. Liu and L. Li, "Influence of fineness on the cementitious properties of steel slag," *Journal of Thermal Analysis and Calorimetry*, vol. 117, no. 2, pp. 629–634, 2014.

[5] C. Shi, "Steel slag — its production, processing, characteristics, and cementitious properties," *Journal of Materials in Civil Engineering*, vol. 16, no. 3, pp. 230–236, 2005.

[6] J. N. Murphy, *Recycling Steel Slag as a Cement Additive*, University of British Columbia, Vancouver, Canada, 1961, http://circle.ubc.ca/handle/2429/4326.

[7] J. Li, Q. Yu, J. Wei, and T. Zhang, "Structural characteristics and hydration kinetics of modified steel slag," *Cement and Concrete Research*, vol. 41, no. 3, pp. 324–329, 2011.

[8] Z. Chen, R. Li, and J. Liu, "Preparation and properties of carbonated steel slag used in cement cementitious materials," *Construction and Building Materials*, vol. 283, no. 2, Article ID 122667, 2021.

[9] Y. Kong, P. Wang, and S. Liu, "Microwave pre-curing of Portland cement-steel slag powder composite for its hydration properties," *Construction and Building Materials*, vol. 189, no. 20, pp. 1093–1104, 2018.

[10] O. Gencel, O. Karadag, O. H. Oren, and T. Bilir, "Steel slag and its applications in cement and concrete technology: a review," *Construction and Building Materials*, vol. 283, Article ID 122783, 2021.

[11] P. K. Chamling, S. Haldar, and S. Patra, "Physico-chemical and mechanical characterization of steel slag as railway ballast," *Indian Geotechnical Journal*, vol. 50, no. 2, pp. 267–275, 2020.

[12] N. Palankar, A. U. Ravi Shankar, and B. M. Mithun, "Durability studies on eco-friendly concrete mixes incorporating steel slag as coarse aggregates," *Journal of Cleaner Production*, vol. 129, no. 15, pp. 437–448, 2016.

[13] C. M. Kansal and R. Goyal, "Analysing mechanical properties of concrete with nano silica, silica fume and steel slag," *Materials Today: Proceedings*, vol. 45, no. 94, pp. 4520–4525, 2021.

[14] F. Han and Z. Zhang, "Properties of 5-Year-Old concrete Containing Steel Slag Powder," *Powder Technology*, vol. 334, pp. 27–35, 2018.

[15] G. Liu, K. Schollbach, P. Li, and H. Brouwers, "Valorization of converter steel slag into eco-friendly ultra-high performance concrete by ambient CO2 pre-treatment," *Construction and Building Materials*, vol. 280, no. 7, Article ID 122580, 2021.

[16] Y. F. Li, Y. Yao, and L. Wang, "Recycling of industrial waste and performance of steel slag green concrete," *Journal of Central South University of Technology*, vol. 16, no. 5, pp. 768–773, 2009.

[17] Q. Li, Y. Qiu, A. Rahman, and H. Ding, "Application of steel slag powder to enhance the low-temperature fracture properties of asphalt mastic and its corresponding mechanism," *Journal of Cleaner Production*, vol. 184, no. 20, pp. 21–31, 2018.

[18] W. Jiao, A. Sha, Z. Liu et al., "Study on thermal properties of steel slag asphalt concrete for snow-melting pavement," *Journal of Cleaner Production*, vol. 277, no. 6, p. 123574, 2020.

[19] P. Chaurand, J. Rose, V. Briois et al., "Environmental impacts of steel slag reused in road construction: a crystallographic and molecular (XANES) approach," *Journal of Hazardous Materials*, vol. 139, no. 3, pp. 537–542, 2007.

[20] E. U.-B. R. E. F. Ceramics, "Integrated Pollution Prevention and Control(IPPC)Reference Document on Best Available Techniques in the Ceramic Manufacturing Industry," 2005, https://eippcb.jrc.es/pages/FActivities.htm.

[21] T. Zhang, Q. Yu, J. Wei, J. Li, and P. Zhang, "Preparation of high performance blended cements and reclamation of iron concentrate from basic oxygen furnace steel slag," *Resources, Conservation and Recycling*, vol. 56, no. 1, pp. 48–55, 2011.

[22] J. Geiseler, H. Kollo, and G. E. Lang, "Influence of blast furnace cements on durability of concrete structures," *ACI Materials Journal*, vol. 92, no. 3, pp. 252–257, 1995, https://www.researchgate.net/publication/279897880.

[23] N. R. Buenfeld, J. Bensted and P. Barnes, "Structure and performance of cements," *Engineering Structures*, Spon Press, vol. 251, p. 565, 2nd edition, 2002.

[24] S.-C. Kou, C.-S. Poon, and M. Etxeberria, "Influence of recycled aggregates on long term mechanical properties and pore size distribution of concrete," *Cement and Concrete Composites*, vol. 33, no. 2, pp. 286–291, 2011.

[25] A. Guerrero, S. Goñi, A. Maćias, and M. Luxan, "Mechanical properties, pore size distribution, and pore solution of fly ash-belite cement mortars," *Cement and Concrete Research*, vol. 29, no. 11, pp. 1753–1758, 1999.